JACS
JOURNAL OF THE AMERICAN CHEMICAL SOCIETY
Article
pubs.acs.org/JACS

New Insights into Frustrated Lewis Pairs: Structural Investigations of Intramolecular Phosphane−Borane Adducts by Using Modern Solid-State NMR Techniques and DFT Calculations

Thomas Wiegand,[†] Hellmut Eckert,*[,†] Olga Ekkert,[‡] Roland Fröhlich,[‡] Gerald Kehr,[‡] Gerhard Erker,*[,‡] and Stefan Grimme*[,≠]

[†]Institut für Physikalische Chemie and Graduate School of Chemistry, WWU Münster, Corrensstrasse 30, D 48149 Münster, Germany

[≠]Mulliken Center for Theoretical Chemistry, Institut für Physikalische und Theoretische Chemie, Universität Bonn, Beringstrasse 4, D 53115 Bonn, Germany

[‡]Organisch-Chemisches Institut, WWU Münster, Corrensstrasse 40, D 48149 Münster, Germany

Supporting Information

ABSTRACT: Covalent bonding interactions between the Lewis acid and Lewis base functionalities have been probed in a series of "frustrated Lewis pairs" (FLPs) (mainly substituted vinylene linked intramolecular phosphane−borane adducts), using solid-state nuclear magnetic resonance techniques and accompanying DFT calculations. Both the ^{11}B NMR isotropic chemical shifts and nuclear electric quadrupolar coupling parameters turn out to be extremely sensitive experimental probes for such interactions, revealing linear correlations with boron−phosphorus internuclear distances. The principal component V_{zz} of the ^{11}B electric field gradient tensor is tilted slightly away (~20°) from the boron−phosphorus internuclear vector, leading to an improved understanding of the remarkable reactivity of the FLPs. Complementary ^{31}P{^{1}H}-CPMAS experiments reveal significant ^{31}P−^{11}B scalar spin−spin interactions ($^{1}J \approx 50$ Hz), evidencing covalent bonding interactions between the reaction centers. Finally, ^{11}B{^{31}P} rotational echo double resonance (REDOR) experiments show systematic deviations from calculated curves based on the internuclear distances from X-ray crystallography. These deviations suggest non-zero contributions from anisotropic indirect spin−spin (J anisotropy) interactions, thereby offering additional evidence for covalent bonding.

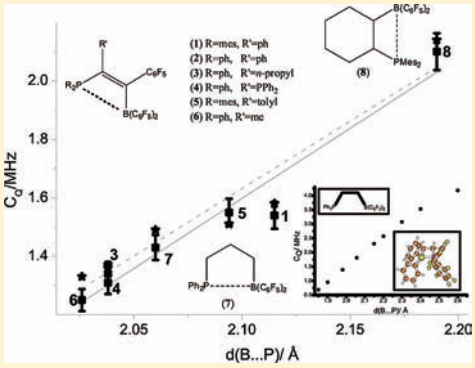

INTRODUCTION

Frustrated Lewis acid/base pairs (FLPs), which feature intramolecular Lewis acid and Lewis base functionalities in close proximity but within constrained geometries, are of great interest in the field of homogeneous catalysis.[1] Their reactivity stems from the presence of bulky, sterically demanding ligands (e.g., mesityl, ^{t}Bu, and C_6F_5 groups) attached to the reactive centers, thereby inhibiting the anticipated Lewis acid/base adduct formation.[2] The close proximity of the Lewis acid and the Lewis base moieties leads to a remarkable cooperative reaction behavior that is in many cases comparable to that of organometallic compounds. The most prominent example is the activation of dihydrogen,[3−7] which offers a completely new line of research for the development of metal-free, environmentally friendly hydrogenation catalysis. But also the activation of CO_2,[8] carbonyl compounds,[9,10] alkenes,[11,12] dienes,[13] and alkynes[14] and the capture of NO[15] have been reported. A large variety of FLPs can be formed from a phosphane Lewis base and a borane Lewis acid functionality combined in an intermolecular[4] or intramolecular manner. Typical adducts (**1**−**9**) as investigated in the present manuscript are shown in Figure 1. Of these, one of the earliest and most reactive examples is the four-membered heterocyclic ethylene-bridged phosphane−borane adduct **9** (see Figure 1).[6] Besides an extremely high reactivity toward dihydrogen, this intramolecular adduct undergoes many other interesting addition reactions.[10] The class of intramolecular phosphane/borane adducts has recently been extended to unsaturated C_2-linked systems, which possess more moderated reactivities.[16] A whole series of these molecules is synthesized by a 1,1-carboboration reaction and therefore represents a new application in the field of P−C bond activation chemistry.

Despite the large number of experimental reports in the field of FLP chemistry, only a few deal with the theoretical understanding of the chemical reaction mechanisms involving these molecules. Pápai[17,18] and Grimme[19] have proposed dihydrogen activation mechanisms, in the latter case implicating especially the polarization of dihydrogen in the electric field generated by the donor/acceptor atoms of the intramolecular adducts. A common structural characteristic of these compounds enforcing cooperative effects is the presence of

Received: October 28, 2011
Published: January 20, 2012

   dx.doi.org/10.1021/ja210160k | J. Am. Chem. Soc. 2012, 134, 4236−4249

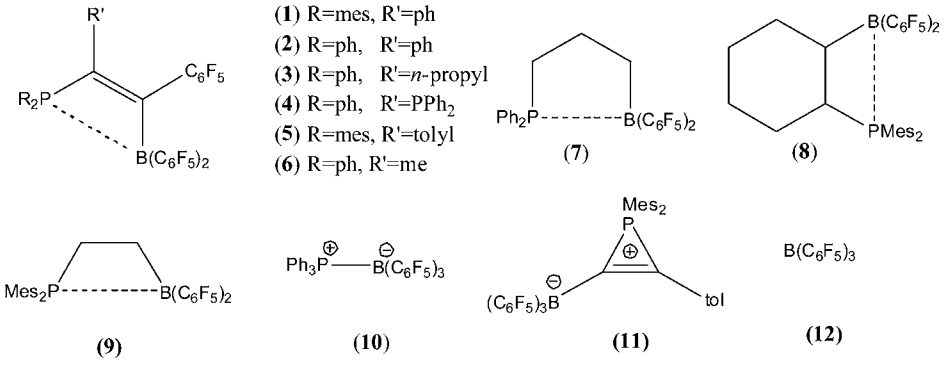

Figure 1. Scheme showing the structures of the investigated compounds.

significant noncovalent interactions among the bulky ligands. In addition the catalytic activity appears to be modulated by weak interactions (of either the covalent or the noncovalent type) between the two reactive centers. The present study introduces modern solid-state NMR techniques, for the first time, as an experimental probe of such interactions for a series of closely related P/B pairs (mainly substituted vinylene-bridged phosphane–borane adducts[16]), in which the internuclear distance can be varied over a comparatively wide range by suitable choice of ligands. We explore compositional trends signifying weak $^{11}B\cdots^{31}P$ covalent interactions by studying the NMR parameters (such as nuclear electric quadrupolar coupling constants, isotropic chemical shifts and indirect spin–spin coupling constants) with the goal of obtaining a deeper structural insight into the reactivity of those molecules.

^{11}B MAS NMR spectroscopy has developed into a well-established tool for the structural characterization of inorganic boron compounds, as well as boranes.[20] Both the ^{11}B chemical shifts, δ_{CS}^{iso}, and quadrupole coupling constants, C_Q, are highly sensitive to the boron coordination number, high-frequency shifts and large C_Q values being associated with trigonally coordinated boron sites and low-frequency shifts and small C_Q values with four-coordinated boron species.[20] Finally, the electric field gradient (EFG) asymmetry parameter, η, characterizes the degree to which the local symmetries of the three- or four-coordinated boron species deviate from the axial symmetries D_{3h} or C_{3v}, respectively. In the present study, we establish ^{11}B magic angle spinning (MAS) NMR in the field of frustrated Lewis pairs and highlight the remarkable sensitivity of its parameters toward even small changes in the surroundings of the boron nuclei in local environments that might be considered between three- and four-coordinated bonding scenarios. As previous works have shown, the ^{11}B EFG tensor is also available with high accuracy by DFT calculations, allowing a visualization of the individual tensor components in the molecular axis frame.[21,22] In a similar vein, the present study examines ^{31}P solid-state NMR parameters such as isotropic chemical shifts and scalar $^{31}P-^{11}B$ spin–spin coupling constants as probes for covalent boron–phosphorus interactions. Finally, we explore the potential and limitations of $^{11}B\{^{31}P\}$ rotational echo double resonance (REDOR)[23] experiments for internuclear distance measurements in these compounds.

The substituted vinylene-bridged intramolecular adducts (compounds **1**–**6** in Figure 1, for a characteristic structure see Figure 2) consist of a heterocyclic, nearly planar four-membered ring structure as present also in the most prominent FLP, **9**.[6] The bridging olefinic functionality leads to an

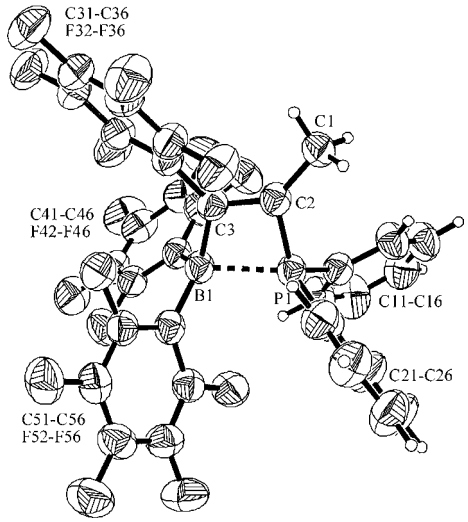

Figure 2. Crystal structure of **6** acting as a representative model for the intramolecular B/P adducts.

extraordinarily rigid backbone of those molecules. In the compounds **7**[24] and **8**,[25] the Lewis acid and base functionalities are linked via a trimethylene and cyclohexylene bridge, respectively. In all molecules, the Lewis acidity of the boron site is enhanced by electron-withdrawing C_6F_5 ligands, while the phosphorus site is electron-rich due to ligands such as mesityl or phenyl. Especially characteristic are significant noncovalent $\pi-\pi$ interactions between the electron-poor and electron-rich arene ligands leading to a further stabilization of these molecules.[19] Compound **10** represents a typical Lewis acid/base adduct,[26,27] while compound **11**[28] acts as a reference material without any interaction between the base and the acid center. Compounds of type **11** are formed at the beginning of the carboboration and are isolated as stable intermediates, while compound **12** represents the borane starting material. In all cases (except **11** and **12**), the Lewis acid and Lewis base moieties are in close contact exhibiting B···P internuclear distances varying between 2.03 and 2.19 Å. Within the series of substituted vinylene-bridged adducts, this distance can be adjusted by choice of the ligands on the phosphorus Lewis base site: the more bulky those ligands are, the larger is the boron–phosphorus distance. While these adducts show some of the typical FLP reactions, they do not activate dihydrogen under standard reaction conditions (i.e., ambient temperature and 60 bar H_2 pressure). Nevertheless, we note that the thermodynamic window for the H_2 activation is extremely small, indicating that their reactivity is already moderated (relative

dx.doi.org/10.1021/ja210160k | J. Am. Chem. Soc. 2012, 134, 4236–4249

to those of **8** and **9**) by weak intramolecular interactions between the centers. In the present study, quantitative information to this effect will be presented based on combined solid-state NMR experiments and DFT calculations.

EXPERIMENTAL SECTION

The synthesis and general characterization of compounds **1**−**12** have been already reported,[6,16,24−29] and relevant details are given in the Supporting Information.

Solid-state NMR measurements were carried out on BRUKER Avance III (300 MHz), Avance DSX 400, and BRUKER Avance DSX 500 spectrometers, corresponding to magnetic flux densities of 7.05, 9.4, and 11.74 T, respectively. All spectrometers were equipped with 4 mm NMR double and triple resonance probes operating at MAS rotation frequencies between 2.4 and 14 kHz.

^{11}B spectra were mainly measured on the 500 MHz spectrometer at a Larmor frequency of 160.5 MHz. Signals were acquired following excitation with 30° pulses about 0.6 μs in length and repetition times ranging between 5 and 30 s. Proton decoupled ^{11}B{^{1}H} spectra were obtained at 9.4 T with 90° pulses of about 1.5 μs length and a ^{1}H decoupling pulse length of 7.1 μs applied in a TPPM-15[30] decoupling scheme. ^{11}B triple-quantum (TQ) MAS NMR spectra[31] were obtained at 11.74 T using a three-pulse z-filtering sequence.[32] The optimized lengths of the strong preparation and reconversion pulses were varied between 3.8 and 5.5 μs and between 1.5 and 1.7 μs, respectively (nutation frequency $\nu_1 \approx 130$ kHz for a liquid sample). The single quantum signal was detected by a soft pulse of 10 μs length in all cases (nutation frequency $\nu_1 \approx 30$ kHz for a liquid sample). The increment for the evolution time was adjusted to $1/(14000 \times 2^n)$ s (with n value of 1, 2, or 3), and a recycle delay of 5−30 s was used. A comparison of the centers of gravity in the isotropic F1 and anisotropic F2 dimensions reveals the isotropic chemical shift, δ_{CS}^{iso}, and the "second-order quadrupolar effect (SOQE)" defined as SOQE = $C_Q(1 + \eta^2/3)^{1/2}$ with C_Q and η representing the nuclear electric quadrupolar coupling constant and the electric field gradient asymmetry parameter, respectively. Those parameters were also determined quantitatively by line shape fitting analysis of the MAS spectra and MQMAS slices using the DMFIT software (version 2011).[33] Chemical shifts are reported relative to a $BF_3{\cdot}Et_2O$ standard.

^{31}P{^{1}H} CPMAS spectra were measured at 9.4 T with ^{1}H 90° pulse lengths of 4−6 μs, a contact time of 5 ms, and a relaxation delay of 5 s. Hartmann−Hahn conditions were adjusted on $NH_4H_2PO_4$. An efficient polarization transfer was achieved by a ramped-amplitude CP step[34] with $\nu_{RF}(^{1}H)$ being swept from 54 to 27 kHz in 64 steps (in the case of a ^{1}H 90° pulse length of 4.6 μs). All spectra were acquired with TPPM-15 proton decoupling during the data acquisition applying decoupling pulses of 6.7−10 μs length (~10/12 π pulses). Additional ^{31}P{^{1}H} CPMAS spectra using the SW-TPPM-15 decoupling scheme[35] were recorded at 7.1 T with a ^{1}H 90° pulse length of 3.5 μs, a contact time of 5 ms and a relaxation delay of 5 s. This decoupling sequence changes the amplitude of the decoupling pulses (optimized for each experiment, approximately 10/12 of the π pulse) in a linear way between 75% and 125% of the initial value.[36] Line shape analysis was done by using the DMFIT software (version 2011). Chemical shifts are reported relative to a 85% H_3PO_4 solution.

^{11}B{^{31}P} REDOR experiments were conducted at 9.4 T with the compensated REDOR scheme using radio frequency power levels corresponding to 180° pulses of 6.5−7.5 μs for ^{11}B and ^{31}P. The phases of the ^{31}P π pulses were alternated according to the XY4 phase cycling scheme.[37] Spinning speeds of 12−14 kHz were used. For creating a reproducible magnetization in each experiment, a saturation comb consisting of 32 90° pulses was applied. Constant-time-REDOR (CT-REDOR) experiments[38] (also with compensation) were performed under similar experimental conditions with spinning speeds of 5 and 10 kHz, respectively. The simulations of both CT-REDOR and REDOR curves were carried out with the SIMPSON software.[39] For an accurate description of the oscillatory part of the REDOR curves, the REPULSION powder angle averaging scheme (rep2000)[40] was applied and 36 equally spaced gamma angles were used. Experimentally determined chemical shift anisotropy (CSA) parameters were included in the simulations (for details see Figure S1, Supporting Information). All the simulations utilize magnetic B···P dipole−dipole coupling constants calculated from the B···P internuclear distances extracted from the crystallographic information available.

Ab Initio Calculations. All calculations were carried out using the program packages TURBOMOLE (version 6.0 and 6.3)[41,42] and GAUSSIAN (version GAUSSIAN09).[43] The geometry optimizations have been performed on a DFT meta-GGA (TPSS[44]) level of theory (starting with the crystal structure if available) applying the recently developed D3 dispersion correction[45] and Ahlrich's def2-TZVP[46] basis set. All geometry optimizations were performed within the TURBOMOLE program suite. In all TURBOMOLE SCF calculations, an energy convergence criterion of 10^{-7} E_h was chosen, and in all geometry optimizations, an energy convergence criterion of 5×10^{-7} E_h was chosen. The integration grid was set to m4,[47] and the RI approximation[48,49] was used.

For the calculations of nuclear electric quadrupole coupling tensors,[21,50] the positions of the heavy atoms were taken from the crystal structure, whereas the positions of the hydrogen atoms were optimized on the DFT TPSS level with Ahlrich's def2-TZVP basis set. The calculations of the electric field gradients were performed on a GGA DFT level (functional B97-D[51]) using the program package GAUSSIAN09. The def2-TZVP basis set obtained from the EMSL database[52,53] was modified in such a way that tighter basis functions on the boron atom (extracted from the cc-pCVTZ basis set,[54,55] for details see Supporting Information section) were included for having a more accurate description of the region near the boron nucleus. The GAUSSIAN output files were analyzed by using the program EFGShield,[22] version 2.2, for determination of C_Q and η values and visualizing the orientation of the electric field gradient tensor in the molecular geometry by using the DIAMOND software.[56]

In case of model adduct calculations as a function of the boron−phosphorus distance, the latter was fixed to characteristic values ranging between 1.85 and 2.6 Å, while the rest of the structure was optimized on the TPSS-D3 def2-TZVP level of theory; C_Q and η values were calculated at the B97-D/def2-TZVP level of theory.

The magnetic shielding calculations were performed within the GIAO (gauge-independent atomic orbitals) framework.[50,57] For ^{11}B, magnetic shieldings were calculated on the B3-LYP[58,59] and BP-86[60,61] level of theory with the def2-TZVP basis set using the TURBOMOLE program package. Chemical shifts are referenced to $BF_3{\cdot}Et_2O$ by using B_2H_6 ($\delta(B_2H_6)$ = 16.6 ppm vs $BF_3{\cdot}Et_2O$) as an external standard ($\sigma^{BP\text{-}86}(B_2H_6)$ = 81.04 ppm, $\sigma^{B3\text{-}LYP}(B_2H_6)$ = 84.23 ppm).[62−65] ^{31}P chemical shifts were calculated with the B3-LYP functional and the def2-TZVP basis set. Chemical shifts were referenced to phosphoric acid ($\sigma^{B3\text{-}LYP}$ = 274.31 ppm). ^{31}P chemical shift anisotropy (CSA) parameters were calculated on the B3-LYP TZVP[66] level of theory using the program package GAUSSIAN09.

^{31}P/^{11}B indirect spin−spin coupling constants were calculated on a B3-LYP TZVP level of theory using the program package GAUSSIAN09. The same geometries as in the calculations of nuclear quadrupole couplings were used. In case of the *trans* model of **1**, a complete geometry optimization was carried out on the TPSS-D3/def2-TZVP level of theory. The analysis of the distance-dependence of the ^{1}J spin−spin coupling constant for compound **10** was performed by varying the boron−phosphorus distance within the framework of the crystal structure.

Wiberg bond order indices[67] in the Cartesian atomic orbital (CAO) basis were calculated from the TPSS Kohn−Sham determinants by using the TURBOMOLE program package and those in the natural atomic orbitals (NAO) basis were calculated by using the NBO program (version 3.1)[68] as included in GAUSSIAN09.

RESULTS AND DISCUSSION

^{11}B MAS NMR and DFT Calculations. Figure 3 summarizes the ^{11}B MAS NMR data obtained on the intramolecular adducts studied as well as on the reference

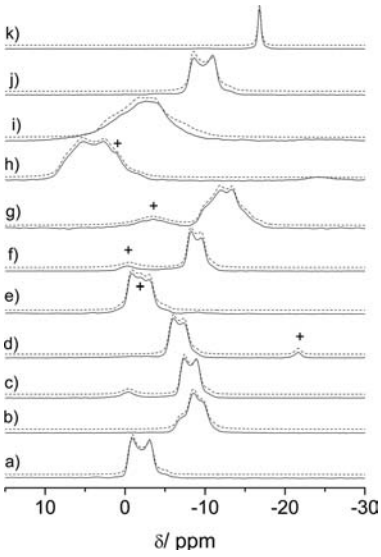

Figure 3. ^{11}B MAS NMR spectra for the investigated P/B compounds (straight lines) and their corresponding simulations (dashed lines): (a) **1** (R = mes, R′ = ph), (b) **2** (R = ph, R′ = ph), (c) **3** (R = ph, R′ = *n*-propyl), (d) **4** (R = ph, R′ = PPh_2), (e) **5** (R = mes, R′ = tolyl), (f) **6** (R = ph, R′ = me), (g) **7**, (h) **8**, (i) **9**, (j) **10**, and (k) **11**. All spectra were acquired at 11.7 T, except g and i, which were measured at 9.4 T under TPPM-15 proton decoupling. The + sign marks impurities.

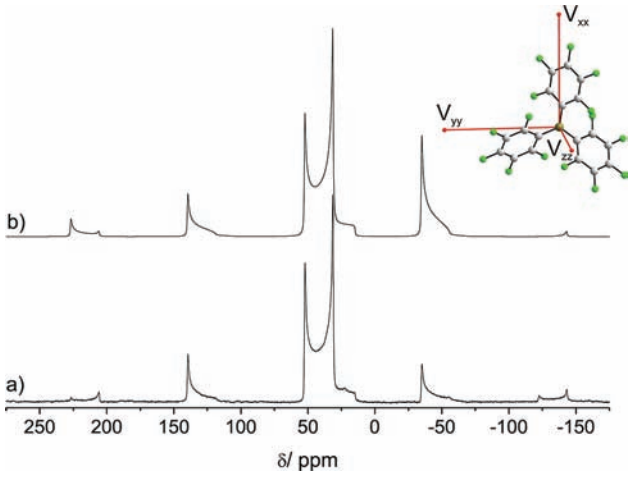

Figure 4. ^{11}B MAS NMR spectrum of the educt of the 1,1-carboboration, $B(C_6F_5)_3$ (**12**), acquired at 11.7 T with a rotation frequency of 14 kHz (a) and simulated spectrum using the SIMPSON program package (b) assuming a C_Q of 4.3 MHz, an η value of 0.02, and $\Delta\sigma$ = 300 ppm. The inset on top shows the DFT calculated (B97-D, def2-TZVP (modified), see Experimental Section) orientation of the EFG in the molecular axis frame. V_{zz} is oriented perpendicular to the boron coordination plane.

materials **10** and **11**. Isotropic chemical shifts, as well as C_Q and η values determined from these data, either by simulating the central transition line shapes using DMFIT[33] and SIMPSON[39] codes or by analyzing the relevant F1 cross sections along the F2 dimensions of 2-D triple-quantum (TQ) MAS NMR spectra,[31,32] are summarized in Table 1. TQMAS experiments are particularly useful for the analysis of spectra with overlapping signals. The reference compound data in particular indicate the large variations in the ^{11}B NMR line shapes that are in principle possible in these systems. Trispentafluorophenylborane ($B(C_6F_5)_3$), **12**, shows a line shape that is strongly affected by second-order quadrupolar effects characterized by a large quadrupolar coupling constant (4.3 MHz) and an asymmetry parameter close to zero (see Figure 4 and Figure S2, Supporting Information). As previously noted by Bryce et al. for related compounds (e.g., trimesitylborane, $BMes_3$, and triphenyl borate, $B(OPh)_3$), the second-order quadrupolar perturbation line shape of the MAS center band is significantly affected by a large chemical shift anisotropy.[20] While the crystal structure of $B(C_6F_5)_3$ is not known, the characteristic ^{11}B MAS NMR line shape is consistent with a local D_{3h} symmetry at the boron center, as expected from the fact that all three ligands are identical. The DFT calculation of the ^{11}B electric field gradient in the gas phase yields a C_Q value of 4.04 MHz and an η value of zero, which is in good agreement with the experimental results obtained in the solid state. The principal EFG component, V_{zz}, is aligned perpendicular to the molecular plane. The simulation that best reproduces the experimental spectrum indicates that the electric field gradient tensor at the ^{11}B site and the ^{11}B magnetic shielding tensors are coincident. The four-coordinated boron atom of compound **11** exhibits the

Table 1. Experimentally and Quantum-Chemically Determined ^{11}B δ_{CS}^{iso}, C_Q, and η Values[a]

	δ_{CS}^{iso} (expt, ppm, ±0.5)	C_Q (expt, MHz, ±3%)	η (expt, ±0.1)	δ_{CS}^{iso} (calcd, ppm)	C_Q (calcd, MHz)	η (calcd)	angle (V_{zz}, B, P; deg)[f]
1	0.3[b]	1.54[c]/1.55[b]	0.19[b]	−0.6	1.58	0.12	22.4
2	−7.6[b]; −5.9[b]	1.25[b]; 1.36[b]	0.18[b]; 0.15[b]	−7.4[e]	1.43[e]	0.05[e]	21.6[e]
3	−6.6[b]	1.34[c]/1.35[b]	0.15[b]	−7.6	1.37	0.04	23.2
4	−4.7[b]	1.31[c]/1.31[b]	0.15[b]	−6.6	1.36	0.05	24.2
5	0.3[b]	1.55[c]/1.57[b]	0.17[b]	−1.9	1.51	0.13	23.7
6	−7.5[b]	1.25[c]/1.27[b]	0.16[b]	−9.2	1.33	0.07	22.8
7	−9.1[c]	1.43[c]	0.55[c]	−10.2	1.49	0.53	8.5
8	8.6[c]	2.10[c]	0.43[c]	7.3	2.14	0.39	20.0
9	3.3[c]	1.8[c]	0.6[c]	14.6[e]	2.62[e]	0.26[e]	19.2[e]
10	−7.4[c]	1.59[c]/1.63[b]	0.15[b]	−8.8	1.60	0.02	0.5
11	−16.7[c]	0.33[d]	0.3[d]	−19.5	0.47	0.4	
12	58.7[c]	4.26[c]	0.02[c]	54.5[e]	4.04[e]	0.00[e]	

[a]Chemical shifts were calculated on a DFT B3-LYP/def2-TZVP, electric field gradients on a DFT B97-D/def2-TZVP (modified) level of theory. [b]Determined from line shape analysis of slices from MQMAS experiments. [c]Determined from line shape analysis of ^{11}B MAS spectra. [d]Determined from ^{11}B SATRAS spectrum (see Figure S3, Supporting Information). [e]Fully geometry-optimized structures are used within the calculations. [f]Orientation of the DFT calculated (B97-D, def2-TZVP (modified)) main principal component of the EFG tensor, V_{zz}, expressed by the angle between this parameter and the B···P distance vector.

dx.doi.org/10.1021/ja210160k | J. Am. Chem. Soc. 2012, 134, 4236−4249

Table 2. Comparison of Crystallographic B···P Distances and Bond Angle Sums around B of the Investigated Compounds with Theoretical Values from a Full DFT Geometry Optimization on the TPSS Level of Theory (Basis def2-TZVP) Using the Recently Developed D3 Dispersion Correction

	d_{cryst}(B···P), Å	d_{calc}(B···P), Å	angle sum B(cryst), deg	angle sum B(calcd), deg
1	2.115(2)	2.130	344.1(2)	346
2	*a*	2.046	*a*	352
3	2.038(3)	2.046	349.2(2)	351
4	2.038(7)	2.047	348.1(5)	350
5	2.094(2)	2.131	342.1(1)	346
6	2.026(2)	2.046	349.0(2)	351
7	2.060(2)	2.079	342.4(2)	345
8	2.188(5)[b]/2.206(5)	2.174	344.2(4)/343.8(4)	344
9	*a*	2.261	*a*	352
10	2.180(6)	2.221	339.9(4)	343
11	3.257(6)[b]/3.232(5)	3.234	326.5(4)/329.0(4)	334

[a]No crystal structure available. [b]Used within the DFT calculations.

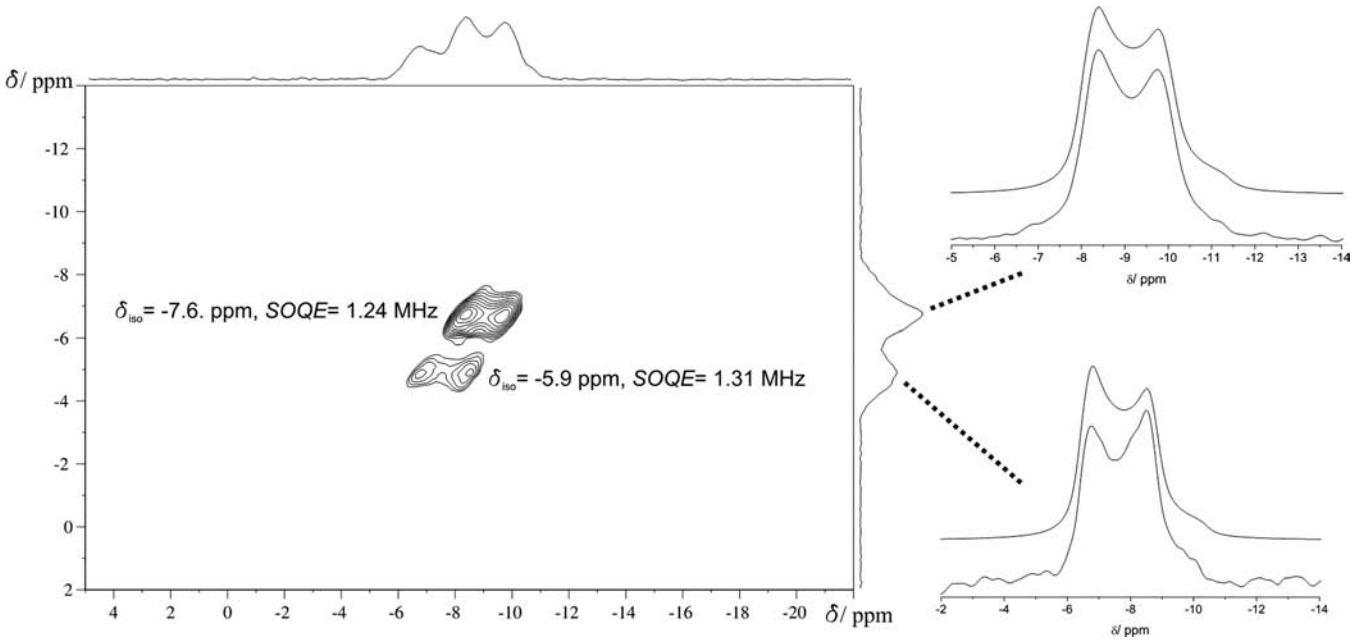

Figure 5. ^{11}B TQ-MAS spectrum (left) of the phosphane–borane adduct **2** (R = ph, R′ = ph) and corresponding 1D slices along F2 (right) performed at 11.7 T with a spinning frequency of 14 kHz. The spectrum shows two slightly different resonances with isotropic chemical shifts of −7.6 ppm and −5.9 ppm, respectively, with a SOQE of 1.24 and 1.31 MHz, respectively. The corresponding experimental F1 slices and their simulations are shown on the right.

smallest quadrupolar coupling constant within this series (0.33 MHz, η = 0.3), reflecting a boron site with nearly tetrahedral symmetry. These values were determined by fitting the intensity distribution within the MAS side band pattern, which arises from the effect of magic-angle spinning on the anisotropically broadened first-order quadrupolar satellites (SATRAS, see Figure S3, Supporting Information). Finally, the spectrum of the PPh_3–$B(C_6F_5)_3$ adduct **10** is characterized by an intermediate quadrupolar coupling constant (1.6 MHz) and an asymmetry parameter close to zero, consistent with the local C_{3v} symmetry of the central boron atom. The trimethylene-bridged phosphane–borane adduct **7** shows a characteristic ^{11}B MAS NMR line shape reflecting a quadrupolar coupling constant of 1.4 MHz and an asymmetry parameter of 0.55. In this case, the large asymmetry parameter can be attributed to the unsymmetric ligation pattern (C_6F_5 groups and the trimethylene bridge) and the significant interaction with the phosphorus Lewis base center evident from the crystal structure.

The remaining spectra shown in Figure 3 reveal the wide range of chemical shifts and quadrupolar interaction parameters measured for the different intramolecular adducts investigated in this study. The phosphane–borane systems **1**–**6** and the PPh_3–$B(C_6F_5)_3$ Lewis acid/base adduct **10** give rise to intermediate quadrupolar coupling strengths (C_Q values near 1.5 MHz) thus clearly reflecting the local distortions from the ideal trigonal local geometry present in **12**. The latter distortions are also readily apparent from the angle sums, obtained from both the DFT calculations and the crystal structures (see Table 2). Notably, the distortions appear to maintain the local C_3 axis, as reflected by the calculated and measured asymmetry parameters, which are found close to zero. The isotropic chemical shift values range within the interval 0.3 to −7.6 ppm. The agreement with the theoretically calculated values is excellent (R^2 = 0.998, see Table 1 and

Figure S4, Supporting Information). For compound **2**, the TQMAS spectrum clearly shows two slightly different boron positions (C_Q = 1.25 and 1.36 MHz, δ_{CS}^{iso} = −7.6 and −5.9 ppm) in an approximate intensity ratio of 2:1 (see Figure 5 and Figure S5, Supporting Information). We believe that these different sites might arise from packing effects or disorder in the solid state, which may explain why up to now the crystal structure could not be solved. Our unconstrained DFT geometry optimizations (TPSS-D3,[44,45] def2-TZVP,[46] see Experimental Section) yield a boron−phosphorus distance of 2.05 Å, which is in good agreement with the experimentally determined distances within the series of intramolecular adducts (see Table 2). Finally, relatively large C_Q values are measured for the extremely reactive model compounds **8** and **9**. In these cases, the asymmetry parameters of 0.43 and 0.6 reflect the considerable distortion of the electric field gradient caused by the nonsymmetric substitution pattern at the three-coordinated boron site. In the case of compound **9**, the experimental ^{11}B chemical shifts and quadrupolar coupling parameters show sizable deviations from the calculated values. This might reflect the more fluxional character of this compound in the solid state. As a result, a correct calculation would have to include an averaging process over multiple configurations, which was not done in the present study.

The interesting question is whether the ^{11}B chemical shifts and quadrupolar coupling parameters can be related to special structural characteristics that define the high reactivity of FLPs and therefore may allow further insights into the reaction behavior of those molecules. As previous calculations have shown,[19] the electric field generated by the Lewis acid and Lewis base functionality is responsible for the extremely fast heterolytic cleavage of dihydrogen. Moreover, these calculations have revealed that the dissociation of the H_2 molecule takes place nearly barrier-free after the molecule is oriented within the reactive pocket. Therefore, it is reasonable to assume that the boron−phosphorus distance is a very important structural characteristic having a significant influence on the reactivity of these molecules. Our investigations show that the ^{11}B NMR parameters for compounds **1**−**8** are strongly correlated with this parameter. Figure 6 illustrates the high sensitivity of ^{11}B isotropic chemical shifts to the B···P distances for the series of these intramolecular adducts. The general trend that larger distances result in a high-frequency shift of the ^{11}B resonance is clearly apparent. The data are compared with chemical shift calculations carried out for the model compound $Ph_2P-C_2H_4-B(C_6F_5)_2$, where the boron−phosphorus distance was changed from 1.8 to 2.6 Å and full relaxation of all other degrees of freedom was guaranteed. The closely parallel chemical shift trends observed for the experimental and theoretical data clearly confirm these correlations.

Besides the chemical shifts, especially, the ^{11}B C_Q values are modified by the intramolecular interactions between the Lewis centers. These effects are summarized in Figure 7 in which the C_Q values are plotted against the experimental B···P distances for the compounds **1**−**8**. The smallest quadrupolar coupling constants are observed for the intramolecular adduct **6**, while the largest C_Q results in case of compound **8**. Figure 7 points out that the larger the B···P distances are, the larger are the C_Q values indicating lesser degrees of distortion of the boron site from trigonal geometry. These results suggest that the ^{11}B quadrupolar coupling constant can be interpreted in terms of the interaction between the Lewis acid and Lewis base functionality. Again, theoretical investigations on the model

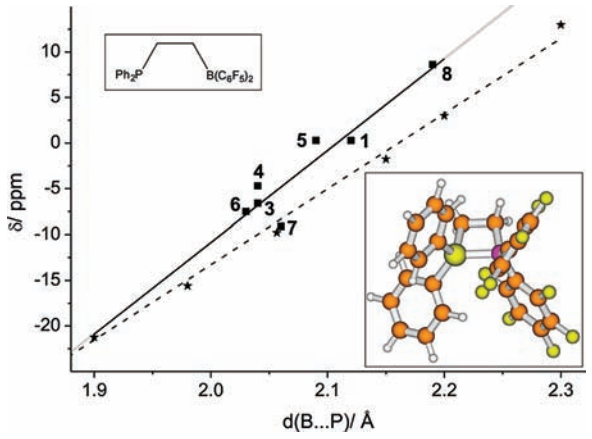

Figure 6. Correlation between experimentally determined ^{11}B chemical shifts in case of the bridged B/P adducts (■) and in case of DFT calculations (chemical shifts on the BP-86/def-TZVP level of theory) for a model compound (see inset) with different B···P distances (★, for technical details see Experimental Section). Larger B···P distances result in a stronger deshielding of the boron atom. The straight line represents a linear regression for the experimental values (R^2 = 0.85) and the dashed line for the DFT calculated values using the model system (R^2 = 0.99). Compound **9** is omitted from the correlation because of its fluxional character and because no experimental B···P distance is known, and compound **10** is excluded, because the computational model is inadequate for this molecule, where both B and P are bound to three aromatic ligands.

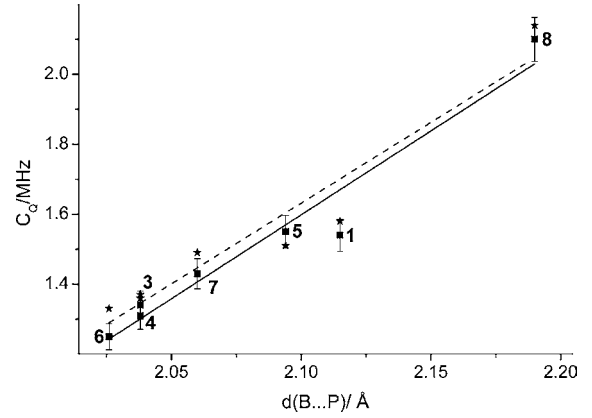

Figure 7. Correlation between experimentally determined (■, from line shape analysis of ^{11}B MAS experiments) and DFT-calculated (B97-D/def2-TZVP (modified), ★) ^{11}B C_Q values and boron−phosphorus distances: larger B···P distances result in larger C_Q values due to less distortion from trigonal geometry at the boron site. The error bars indicate an experimental uncertainty of about 3%. The straight line shows a linear regression for the experimental values (R^2 = 0.94) and the dashed line a linear regression for the DFT-calculated values (R^2 = 0.91). Compound **9** is omitted from the correlation, because of its fluxional character (see text) and because no experimental internuclear distance is available. Compound **10** is omitted from the correlation, because it does not represent an intramolecular adduct.

system $Ph_2P-C_2H_4-B(C_6F_5)_2$ over the distance range 1.8−2.6 Å confirm these findings: larger quadrupolar coupling constants result for larger B···P distances due to reduced Lewis acid/Lewis base interactions (Figure 8b). These calculations also show that the asymmetry parameter tends to decrease strongly as a function of B···P distances (Figure 8a).

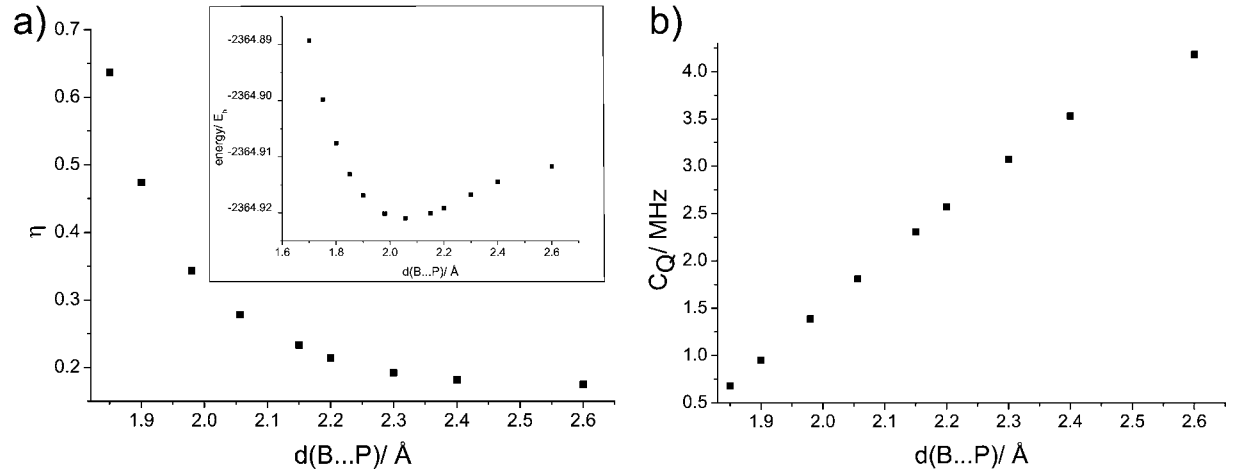

Figure 8. DFT calculations of quadrupolar coupling parameters (B97-D, def2-TZVP) for a model compound (see inset of Figure 6) with varying boron−phosphorus distances from 1.8 to 2.6 Å (for details, see Experimental Section) illustrating the correlations between the B···P distance and the asymmetry parameter η (a) and the quadrupolar coupling constant C_Q (b). The data highlight the fact that larger B···P distances result in a smaller distortion of the boron site from trigonal geometry leading to larger C_Q and smaller η values. The inset in panel a shows the potential energy curve with a minimum at 2.06 Å for the TPSS-D3/def2-TZVP level of theory.

A more profound understanding of the experimentally observed correlations of the EFG with the boron−phosphorus distance is obtained by visualizing the DFT-calculated EFG principal axis tensor elements in the molecular frame. In case of main group elements such as boron, the EFG is dominated by the outer core and valence shell electronic distribution.[21] Therefore an accurate description of both the valence and the core shell electrons is required. To this end, we used Ahlrich's def2-TZVP[46] basis set, which is modified at the boron atom by using tighter basis functions extracted out of Dunning's correlation consistent basis set[54,55] (for more details, see Experimental Section and Figure S6, Supporting Information). Our theoretical studies are based on calculations in the gas phase, thus neglecting the interactions between the discrete molecular units in the solid state. As indicated in Figure 9, the DFT B97-D[51] level of theory allows a very accurate determination of ^{11}B C_Q values resulting in a linear correlation between experimentally and theoretically determined values (the R^2 value is determined as 0.997). The theoretical studies reveal in case of the substituted vinylene-linked intramolecular adducts asymmetry parameters ranging between 0.04 and 0.13. These values are consistent with a local boron geometry that is still close to trigonal as is expected from the crystallographically determined bond angle sum for the boron site of about 340−350°.

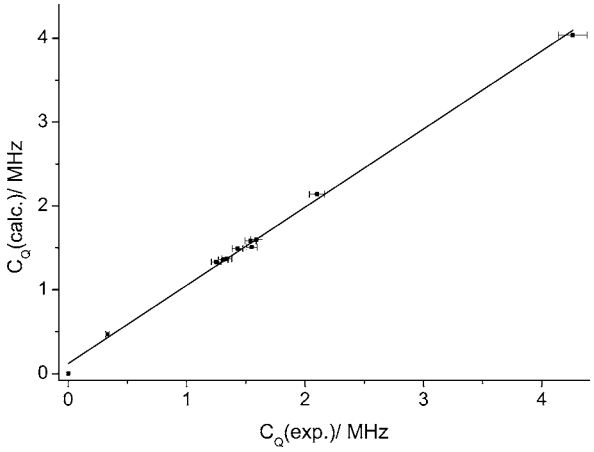

Figure 9. Correlation between experimentally (from ^{11}B MAS NMR experiments) and theoretically (DFT, B97-D, def2-TZVP (modified)) determined C_Q values with an R^2 value of 0.997 and a slope of 0.93. The deviation from unity is partly attributed to uncertainties in the experimental values (estimated at ±3%, see error bars). Compound **9** is not included in this correlation because of the complications arising from its fluxional character (see text).

The strong distance-dependence of the ^{11}B quadrupolar coupling constant can be understood by analysis of the orientation of the largest principal component of the electric field gradient tensor in the molecular frame. In all cases, the V_{zz} component points only slightly away from the B···P vector (for examples, see Figure S7, Supporting Information, exact values are given in Table 1) and is therefore strongly influenced by the interaction among both Lewis centers. The herein developed combination of experimental and theoretical NMR work allows an analysis of the electric field described in the theoretical work by Grimme and co-workers in terms of the electric field gradient from the viewpoint of the boron site. Since the calculated principal component of the electric field gradient points slightly away from the boron−phosphorus axis (see Table 1), it is reasonable to assume that a completely linear geometry of the P−H−H−B unit (as, for example, proposed by Pápai and co-workers[17]) is not necessarily an essential requirement for an efficient activation of H_2 within the FLP.[19] These considerations hold also for the adducts **8** and **9**, which are extremely sensitive toward a reaction with H_2.

^{31}P{^{1}H} CPMAS NMR and DFT Calculations. Figure 10 summarizes the ^{31}P{^{1}H} CPMAS NMR spectra of the intramolecular adducts of our present study, and Table 3 summarizes the spectroscopic parameters determined from them. The ^{31}P isotropic chemical shifts fall within a narrow characteristic chemical shift window between approximately 25 and 5 ppm directly reflecting the extent of the intramolecular adduct formation. In case of the system **4**, two signals are observed at 24.5 and −8.3 ppm because there are two crystallographically distinct phosphorus positions: one interacting with the boron Lewis acid site and the other one standing

dx.doi.org/10.1021/ja210160k | J. Am. Chem. Soc. 2012, 134, 4236−4249

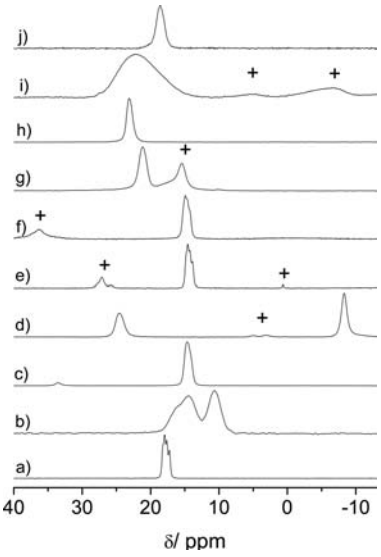

Figure 10. $^{31}P\{^{1}H\}$ CPMAS NMR spectra acquired at 9.4 T with a spinning frequency of 10 kHz applying the TPPM-15 decoupling scheme for the following phosphane−borane adducts: (a) **1** (R = mes, R′ = ph), (b) **2** (R = ph, R′ = ph), (c) **3** (R = ph, R′ = *n*-propyl), (d) **4** (R = ph, R′ = PPh_2), (e) **5** (R = mes, R′ = tolyl), (f) **6** (R = ph, R′ = me), (g) **7**, (h) **8**, (i) **9**, and (j) **10**. All the spectra were acquired at 9.4 T under TPPM-15 proton decoupling. The + sign marks impurities.

apart. As illustrated by Figure S8, Supporting Information, both phosphorus species can be unambiguously differentiated by $^{31}P\{^{11}B\}$ REDOR measurements because the B···P internuclear distances (2.04 vs 4.25 Å) differ significantly: at the chosen dipolar evolution time (0.4 ms), only the resonance at 24.5 ppm is attenuated upon ^{11}B dipolar recoupling. The assignment of this resonance to the adduct-forming moiety is supported by DFT magnetic shielding calculations on the B3-LYP level of theory leading to chemical shifts of 23.6 ppm and −10.1 ppm for both respective resonances.

In the case of the P/B pair **2**, two different peaks with slightly different chemical shifts are observed. Consistent with the conclusions from ^{11}B MAS NMR, this observation confirms the assumed disorder phenomenon suspected in the solid state.

In case of the intramolecular adducts **1**, **3**, **5**, and **6**, the ^{31}P spectra resolve a clear multiplet structure. As illustrated in Figure 11 for compound **1**, the peak splittings are nearly field independent on a hertz scale and therefore suggest the influence of indirect $^{31}P\cdots^{10}B/^{11}B$ spin−spin couplings. In addition, the asymmetric peak separations exhibit the clear signature of dipolar interactions with a quadrupolar nucleus. It is well-known that heteronuclear dipole−dipole interactions of spin-1/2 with nuclei experiencing strong quadrupolar coupling constants are not completely eliminated under MAS conditions.[69] In the context of first-order perturbation theory, the ^{31}P MAS NMR transitions in the presence of this interaction can be written as:

$$\upsilon_m = -m|J| - \frac{S(S+1) - 3m^2}{S(2S-1)}d \quad (1)$$

wherein J are the isotropic $^{10/11}B$, ^{31}P indirect spin−spin coupling constants, S are the nuclear spin quantum numbers for the quadrupolar nuclei (I = 3/2 and 3 for ^{11}B and ^{10}B, respectively), m are the orientational quantum numbers, and d is the residual dipolar coupling.[70,71] The latter value is given by:

$$d = \frac{-3C_Q\left(D - \frac{\Delta J}{3}\right)}{20\nu_s}[3\cos^2\beta^D - 1 + \eta\sin^2\beta^D\cos 2\alpha^D] \quad (2)$$

with D describing the B,P direct dipolar coupling constant, ΔJ the anisotropy of the indirect spin−spin coupling tensor, ν_s the ^{10}B or ^{11}B Larmor frequency, C_Q the ^{10}B or ^{11}B quadrupolar coupling constant, η the asymmetry parameter, and α^D and β^D the Euler angles defining the orientation of the dipolar vector in the principal axis system of the EFG.[72] To the best of our knowledge, we report the first fully resolved asymmetric splitting for a $^{11}B,^{31}P$ spin system, although many other examples of scalar couplings between spin 1/2 and quadrupolar nuclei have been published including the $^{31}P/^{69,71}Ga$,[72] $^{31}P/^{55}Mn$,[73] $^{31}P/^{63,65}Cu$,[74−76] $^{31}P/^{99,101}Ru$,[77] and $^{31}P/^{95,97}Mo$[78] spin systems. Partially resolved J-multiplets in $^{31}P,^{11}B$ spin systems have been previously published.[79,80] The line shape analysis is achieved by using the DMFIT software (see Table 3 and Figure S9, Supporting Information). Our simulations take into account the natural abundances of ^{10}B and ^{11}B, 19.9% and

Table 3. ^{31}P Isotropic Chemical Shifts, Indirect $^{10/11}B-^{31}P$ Spin−spin Coupling Parameters, Residual Dipolar Couplings, and Chemical Shift Anisotropy Parameters (Determined by Line Shape Analysis of Slow-Spinning MAS Experiments) for the Investigated Compounds[a]

	δ_{iso}, ppm	$J(^{31}P,^{11}B)$ ± 5, Hz	$\lvert\Delta\sigma\rvert$, ppm (η_σ)	$J(^{31}P,^{10}B)$, Hz	$J(^{31}P,^{11}B)$, Hz, calcd	$d(^{31}P,^{11}B)$ ± 3, Hz	$d(^{31}P,^{10}B)$ ± 3, Hz	δ_{iso}, ppm, calcd	$\lvert\Delta\sigma\rvert$, ppm (η_σ), calcd
1	17.8	54.5	83.8 (0.49)	18.0	51.1	−5.5[b] (−4.1[c])	−11.5[b] (−8.6[c])	24.1	90.0 (0.40)
2	∼15.3/10.7				47.1			17.0	60.6 (0.19)
3	14.5	52.0	54.0 (0.56)	17.2	51.4	−6.0[b] (−4.5[c])	−12.5[b] (−9.4[c])	16.5	59.7 (0.32)
4	24.5/−8.3		68.2/87.5 (0.77/0.95)		52.4			23.6/−10.1	71.1/72.9 (0.66/0.89)
5	14.4	52.9	94.4 (0.56)	17.5	56.1	−6.0[b] (−4.5[c])	−12.5[b] (−9.4[c])	19.3	104.9 (0.48)
6	14.7	52.0	55.6 (0.65)	17.2	53.2	−6.0[b] (−4.5[c])	−12.5[b] (−9.4[c])	11.8	66.7 (0.51)
7	21.1		56.6 (0.85)		45.5			28.8	60.6 (1.00)
8	23.1		78.2 (0.40)		28.7			32.0	80.0 (0.37)
9	21.7		69.9 (0.92)		10.9			38.0	85.6 (0.61)
10	18.6		30.4 (0.83)		49.9			28.1	5.4 (0.28)
11	−130.5		450.3 (0.05)					−161.1	478.2 (0.16)

[a]The calculated J coupling constants, $\Delta\sigma$, and η values result from DFT calculations (B3-LYP, TZVP), in the latter case using the convention $\Delta\sigma = \sigma_{33} - 1/2(\sigma_{11} + \sigma_{22})$, $\eta_\sigma = (\sigma_{22} - \sigma_{11})/(\sigma_{33} - \sigma_{iso})$ and $|\sigma_{33} - \sigma_{iso}| > |\sigma_{11} - \sigma_{iso}| > |\sigma_{22} - \sigma_{iso}|$. Calculated chemical shifts (DFT, B3-LYP, def2-TZVP) are referenced to phosphoric acid. [b]Measured at 7.1 T. [c]Measured at 9.4 T.

dx.doi.org/10.1021/ja210160k | J. Am. Chem. Soc. 2012, 134, 4236−4249

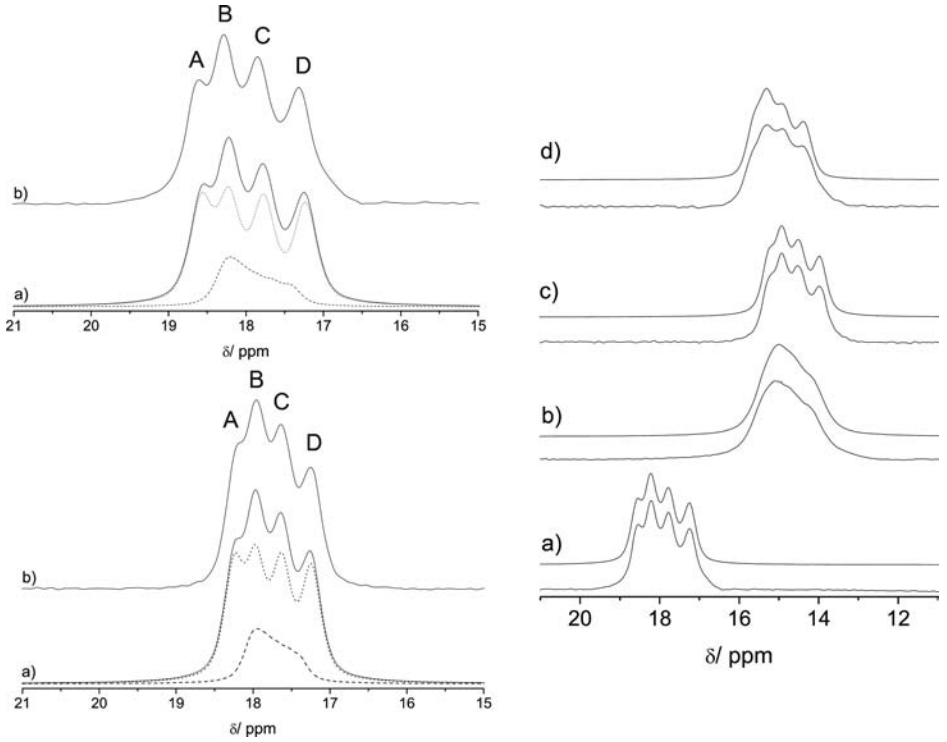

Figure 11. (left) $^{31}P\{^{1}H\}$ CPMAS spectra of compound **1** (R = mes, R′ = ph) acquired at different field strengths. (top) Spectrum measured at 7.1 T using the SW-TPPM-15 decoupling scheme (b) and simulated spectrum (a) showing also the contributions due to $^{31}P\cdots^{11}B$ (dotted line) and $^{31}P\cdots^{10}B$ (dashed line) indirect spin−spin coupling. (bottom) Spectrum measured at 9.4 T using the TPPM-15 decoupling scheme (b) and simulated spectrum (a) showing also the contributions due to $^{31}P\cdots^{11}B$ (dotted line) and $^{31}P\cdots^{10}B$ (dashed line) indirect dipolar coupling. Simulation parameters are given in Table 3. (right) $^{31}P\{^{1}H\}$ CPMAS spectra acquired with the SW-TPPM-15 decoupling scheme at 7.1 T of compounds **1** (a), **3** (b), **5** (c), and **6** (d) where the *J* coupling multiplet could be fully or partially resolved.

80.1%, respectively, and the fact that the *J* and *d* values for ^{10}B and ^{11}B must be scaled according to the magnetogyric ratios ($\gamma(^{10}B)/\gamma(^{11}B)$ = 0.33) and nuclear quadrupole moments ($Q(^{10}B)/Q(^{11}B)$ = 2.084), respectively.[81] Figure 11 shows the $^{31}P\{^{1}H\}$ CP-MAS spectra of **1** at two different field strengths and their corresponding simulations comprising both the contributions from dipolar interactions with ^{10}B and ^{11}B. The simulations reveal that the indirect *J*-coupling between ^{31}P and ^{11}B dominates the line shape splitting and $^{1}J(^{31}P\cdots^{11}B)$ is determined to be 54.5 Hz. This relatively large coupling constant characterizes the covalent interactions between the Lewis acid and Lewis base through a weak but non-negligible covalent bond between boron and phosphorus. It is reasonable to assume that this coupling belongs to a ^{1}J coupling rather than a ^{3}J coupling via the olefinic backbone based on additional evidence discussed in more detail below. Similar splittings are observed for compounds **3**, **5**, and **6** (see Figure 11), whereas in some of the adducts measured in this study, the multiplet splittings are not clearly resolved. We attribute this to degraded resolution owing to a lower degree of sample crystallinity or rapid fluctuations of the spins among the various ^{10}B and ^{11}B Zeeman levels leading to significant relaxation broadening. Nevertheless, even in those cases, field-dependent line width analyses suggest that these interactions contribute to the ^{31}P NMR line shapes observed (see Table 4), except for compound **9**, the line shape of which is dominated by chemical shift distribution effects indicating considerable disorder in the solid state. Additionally the large line width observed for **9** may reflect dynamic processes on the NMR spectra, consistent with its suspected fluxional character in the solid state.

Table 4. ^{31}P Full Widths at Half Maximum (fhwm) at Two Different Field Strengths for Those Molecules for Which the Spin−Spin Coupling Multiplets Could Not Be Resolved[a]

	fhwm (7.0 T), Hz	fhwm (9.4 T), Hz
4 (24.5 ppm)	230	209
4 (−8.3 ppm)	118	119
7	201	186
8	174	152
9	904	1100
10	236	223

[a]Nearly identical peak widths (except for **9**) suggest that spin−spin couplings exert a dominant influence on the line shapes, whereas the broad peak in the case of **9** can be attributed to chemical shift distribution or possibly also dynamic effects. In case of **4**, the remarkable differences in the peak widths directly reflect the influence of ^{1}J and ^{3}J $^{31}P\cdots^{10}B/^{11}B$ spin−spin couplings, respectively, on the MAS NMR line shapes.

The alternative possibility that the observed peak splitting actually arises from ^{3}J, rather than ^{1}J, scalar coupling has been experimentally addressed by analyzing the linewidths of the ^{31}P resonances of **4**. The resonance of the *cis*-phosphorus site interacting with the boron Lewis acid site exhibits a much larger line width than the resonance of the phosphorus site oriented *trans* to the boron unit (209 vs 119 Hz at 9.4 T, see Table 4). This difference is attributed to a much larger ^{1}J coupling constant in comparison to that of a ^{3}J coupling. Additionally, we perfomed theoretical calculations of scalar coupling constants for answering this question satisfactorily. All the *J* coupling analysis described within this work has been

dx.doi.org/10.1021/ja210160k | J. Am. Chem. Soc. 2012, 134, 4236−4249

performed on a hybrid DFT level of theory using the functional B3-LYP.[58,59] For **1**, these calculations lead to a $^{11}B\cdots^{31}P$ J coupling constant of 51.1 Hz, in very good agreement with the experimental value (54.5 Hz). Such values are comparable in magnitude to ^1J ($^{11}B\cdots^{31}P$) values measured in solution for the adduct between PPh_3 and BH_3[79,82] (approximately 60 Hz) and also calculated for the classical Lewis acid/base adduct **10**. Calculations on this model compound under systematic variation of the B···P distance reveal a strong distance dependence, as illustrated in Figure S11, Supporting Information. Finally, the ^3J coupling constant of the *trans* isomer of **1** (see Figure S12, Supporting Information) is calculated as 18.3 Hz. Because this value corresponds to the maximum value based on the Karplus curve[83,84] (dihedral angle of ~180°), a significantly smaller ^3J value would be expected for the *cis*-isomer. Based on all of these considerations, it is safe to conclude that the observed peak splittings arise from ^1J and not from ^3J couplings between ^{31}P and the boron nuclides. This result is in accordance with the computed Wiberg bond-order indices.[67] A bond-order index of about one indicates the presence of a mostly covalent single bond, while values close to zero point to ionic or van der Waals interactions. In the case of the unsaturated intramolecular adducts the Wiberg bond-order indices range between 0.73 and 0.91 in the CAO basis and 0.78 and 0.82 in the NAO basis (see Table S10, Supporting Information). While the WBIs in the CAO basis do not correlate well with the B···P internuclear distances, a much more consistent trend for them is found in the NAO basis, even though individual differences are rather small. The covalent bonding interaction is further probed by a natural bond orbitals (NBO) analysis,[85,86] which reveals a real bond between the phosphorus and boron moieties (see Table S10, Supporting Information) in all of the compounds investigated. The percentage of the NBO on the natural atomic hybrid localized at B correlates well with the B···P internuclear distances, with the highest numbers being observed for compounds **3**, **4**, **6**, and **7** (d(B···P) = 2.02−2.06 Å), intermediate values for compounds **1** and **5** (d(B···P) ≈ 2.09−2.12 Å), and much lower numbers being observed for compounds **8** and **9** (longest distances). Only compound **10** presents a somewhat larger deviation from this trend.

Distance Measurements by $^{11}B\{^{31}P\}$ REDOR Experiments. Against the background of obtaining deeper insight into the interactions between the Lewis acid and base functionalities, it is desirable to determine boron−phosphorus distances even in those compounds for which no crystal structure data are available. Solid-state NMR offers an important opportunity in such cases by conducting rotational echo double resonance (REDOR) experiments. Such REDOR experiments are designed to measure the heteronuclear magnetic dipole coupling constant, D, between two nuclei I and S

$$D = \left(\frac{\mu_0}{8\pi^2}\right) h\gamma_I\gamma_S r_{IS}^{-3} \tag{3}$$

under MAS conditions, where γ_I and γ_S are the corresponding gyromagnetic ratios and r_{IS} is the internuclear distance. While the magnetic dipole−dipole coupling is averaged out over the MAS rotor cycle, it can be reintroduced by applying additional inversion pulse trains to one (or both) of the nuclei during the rotor cycle. This recoupling process diminishes the signal amplitude S, in relation to that observed in the absence of the inversion pulse trains (S_0). Under such conditions, the normalized difference signal $\Delta S = (S_0 - S)/S_0$ changes periodically (like cos $\Delta\Phi$) as a function of the dipolar evolution time, NT_r, where

$$\Delta\Phi = 4\sqrt{2}\,NT_rD \sin\beta\cos\beta\sin\alpha \tag{4}$$

In this expression, N is the number of rotor cycles, T_r is the rotor period, and the angles α and β are Euler angles describing the orientation of the dipolar vector in the MAS rotor axis system. For a polycrystalline sample, a powder average must be taken by appropriate integration over all the Euler angles.

$$\frac{\Delta S}{S_0} = 1 - \frac{1}{4\pi}\int_0^{2\pi} d\alpha \int_0^{\pi} \sin\beta\cos(\Delta\Phi)\, d\beta \tag{5}$$

Equations 4 and 5 yield the so-called REDOR curve, which is a plot of $\Delta S/S_0$ as a function of the dipolar evolution time, NT_r. For a two-spin system, simulation of this curve yields the dipolar coupling constant D from which the internuclear distance r_{IS} can be extracted via eq 3.

The intramolecular adducts of the present study can be considered as ideal $^{31}P-^{11}B$ two-spin systems, for which the internuclear distance should be easily measurable using the REDOR experiment. In the present work, we will demonstrate the calibration of this approach for molecules with known boron−phosphorus distances, which can then be extended to adducts with unknown structures.

Figure 12 shows the $^{11}B\{^{31}P\}$ REDOR curve for **3**. Data have been corrected for potential limitations in the ^{31}P excitation efficiencies, using a compensation scheme developed in our laboratory,[87] applied with a calibration factor of 1.4. As Figure 12 reveals, the data set shows the oscillatory behavior characteristic of an isolated two-spin system as predicted by eqs 4 and 5. The experimental REDOR curve is compared with various simulated curves for different internuclear distances. These REDOR curves are further influenced by the ^{31}P

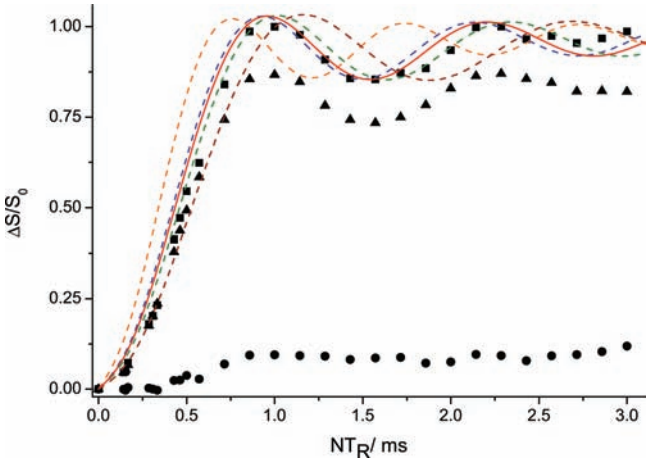

Figure 12. $^{11}B\{^{31}P\}$ compensated REDOR curve (■, calibration factor a = 1.4), REDOR curve (▲), and compensation (●) for the B/P adduct **3** (spinning frequency 14 kHz). SIMPSON simulations assuming a B···P distance of 1.9 Å (orange dashed line), 2.038 Å (crystallographic value, blue dashed line), 2.06 Å (red straight line), 2.1 Å (green dashed line), and 2.2 Å (brown dashed line) are shown. Optimum agreement between the experimental and simulated REDOR curves is achieved by assuming a B···P distance of 2.06 Å. All simulations include the experimental ^{31}P CSA parameters ($\Delta\sigma$ = 54 ppm, η_σ = 0.56).

dx.doi.org/10.1021/ja210160k | J. Am. Chem. Soc. 2012, 134, 4236−4249

chemical shift anisotropy, and the experimentally determined values ($\Delta\sigma$ = 54 ppm, η_σ = 0.56) have been included in these simulations. The oscillating part of the experimental curve is best reproduced by a simulation based on an internuclear distance of 2.06 Å, which differs slightly from the crystallographic value of 2.038 Å. Analogous measurements on the other adducts of the present study show that these underestimations of B···P distances are rather general. The REDOR data tend to underestimate the ^{31}P−^{11}B dipolar coupling strengths systematically, leading to an overestimation of the internuclear distances. Despite this limitation, it will be possible to use REDOR data for obtaining boron−phosphorus internuclear distances for intramolecular adducts with unknown crystal structures or in amorphous systems by calibration against reference data.

As a matter of fact, the experimental and simulated REDOR curves based on the crystallographic B···P distance can be made to agree with each other by including a contribution arising from the J coupling anisotropy (ΔJ) in the simulations (see Figure 13a,b for two representative adducts). As expressed by eq 2, the combination of the direct dipolar coupling and the J anisotropy leads to a reduced effective dipole−dipole coupling, which ultimately determines the frequency of the dipolar oscillations. The determined ΔJ values for the intramolecular adducts range between 60 and 150 Hz; for the adduct **10** a slightly larger value of 200 Hz is observed (see Table 5).

Additionally, we performed ^{11}B{^{31}P} constant-time REDOR (CT-REDOR) experiments in which the evolution time (i.e., the number of rotor periods) is held constant and the positions of the dephasing π-pulses are stepped through the rotation period.[38] Again, these studies were conducted with a compensation scheme. Figure 14 shows compensated CT-REDOR curves for **3** with three different evolution times probing characteristic parts of the REDOR curve. The results support the conclusion drawn for the standard REDOR experiments. The boron−phosphorus distances extracted from the oscillatory part of the CT-REDOR curve tend to be overestimated, and the experimental CT-REDOR curves can be correctly reproduced based on the crystallographic B···P distance if non-zero anisotropies of the J coupling tensor (with ΔJ values ranging between 60 and 219 Hz) are included in the simulations (see Table 5). We emphasize that especially in systems with long ^{11}B relaxation times and low boron contents (by mass), CT-REDOR experiments lead to significant savings in experimental time compared with conventional REDOR measurements.

Finally, for all of the adducts investigated in the present study, we have noticed a subtle distortion of the experimental REDOR and CT-REDOR curves in the sense that the extent of the initial dephasing in the limit of small dipolar evolution times falls slightly below the extent of dephasing predicted from the oscillatory part (see Figure 13). That is, both parts of the REDOR curve would actually result in slightly different values of effective dipolar coupling constants. We speculate that these distortions result mainly from heteronuclear interactions with the homonuclearly coupled proton spin reservoir[88] or other systematic errors as already described in the literature.[89−91] The origin of these deviations can be explored by conducting these REDOR experiments with ^{1}H multipulse decoupling or on perdeuterated compounds, to be examined in future work.

The non-zero contributions of the anisotropy of the J coupling tensor suggested by our REDOR experiments lend further support to the presence of covalent interactions between the acid and base centers in the intramolecular adducts investigated.

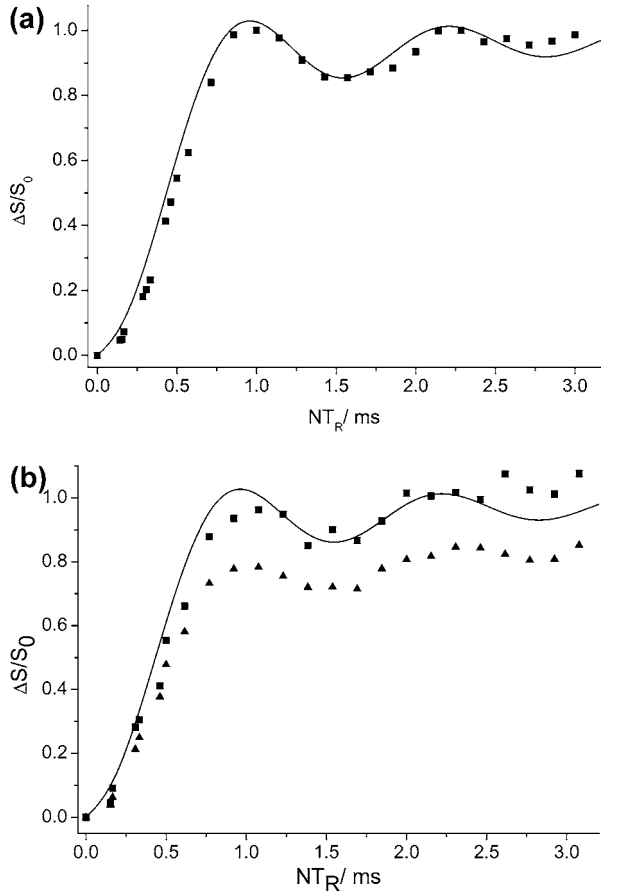

Figure 13. (a) ^{11}B{^{31}P} compensated REDOR curve for the B/P adduct **3** (spinning frequency 14 kHz). The SIMPSON simulation assuming a B···P distance of 2.038 Å (crystallographic value, straight line) is shown. Perfect agreement between the experimental and simulated REDOR curve based on the crystallographic B···P distance can only be achieved if a contribution arising from the J coupling anisotropy (ΔJ) is included in the simulations. The simulation includes the experimental ^{31}P CSA parameters ($\Delta\sigma$ = 54 ppm, η_σ = 0.56) and an assumed J coupling anisotropy of 60 Hz (coincident dipolar and J coupling tensors are assumed). (b) ^{11}B{^{31}P} compensated REDOR curve (■, calibration factor a = 1.3) and REDOR curve (▲) for the B/P adduct **4** (spinning frequency 13 kHz). The SIMPSON simulations assume a three-spin system with B···P distances of 2.038 Å (P1) and 4.25 Å (P2) and include the ^{31}P CSA parameters (P1 $\Delta\sigma$ = 68 ppm, η_σ = 0.77 and P2 $\Delta\sigma$ = 88 ppm, η_σ = 0.95) and an assumed J coupling anisotropy of 60 Hz.

Table 5. B···P Distances from Crystallography and "Best-Fit" Values Obtained from the Oscillatory Part of the ^{11}B{^{31}P} REDOR Curves, Neglecting the Influence of Anisotropic J-Coupling Interactions (ΔJ = 0) and "Best-Fit" Values of ΔJ[a]

	d_{cryst}(B···P), Å	d_{REDOR}(B···P) ($d_{CT\text{-}REDOR}$(B···P)), Å	ΔJ_{REDOR} ($\Delta J_{CT\text{-}REDOR}$), Hz
1	2.115(2)	2.18 (2.14)	150 (60)
3	2.038(3)	2.06 (2.13)	60 (219)
4	2.038(7)	2.06	60
6	2.026(2)	2.06 (2.06)	80 (80)
10	2.180(6)	2.29 (2.29)	200 (200)

[a]Numbers given in parentheses are best-fit values from CT-REDOR data.

dx.doi.org/10.1021/ja210160k | J. Am. Chem. Soc. 2012, 134, 4236−4249

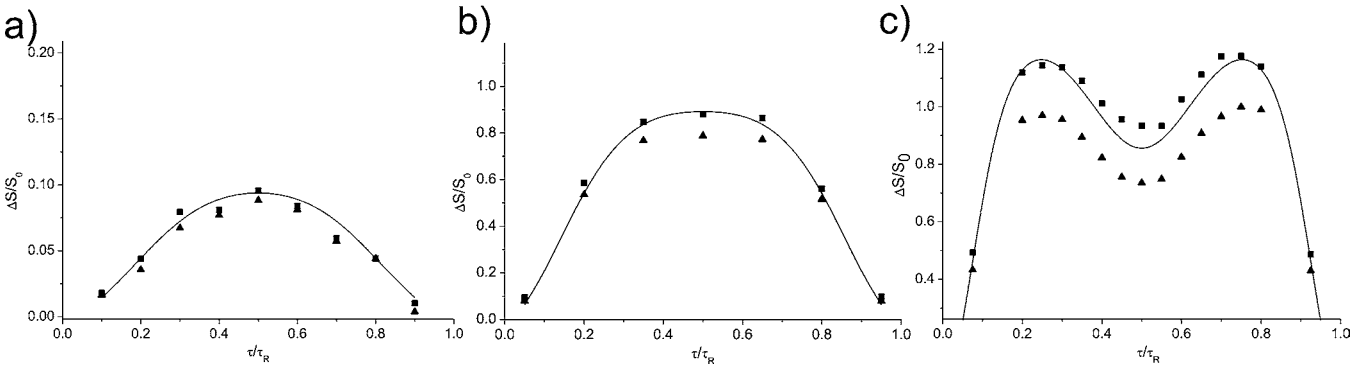

Figure 14. $^{11}B\{^{31}P\}$ compensated CT-REDOR curve (■) and CT-REDOR curve (▲) for the B/P adduct **3** with evolution times of (a) 0.2, (b) 0.8, and (c) 1.6 ms for representing the initial region of a REDOR curve (a) and the oscillatory region (c). Perfect agreement between the experimental and simulated CT-REDOR curves based on the crystallographic B···P distance can only be achieved if a contribution arising from the *J* coupling anisotropy (ΔJ) is included in the simulations. The straight line in panels a and b belongs to SIMPSON simulations assuming a B···P distance of 2.038 Å and using the experimental ^{31}P CSA parameters ($\Delta\sigma$ = 54 ppm, η_σ = 0.56) and a *J* coupling anisotropy of 334 Hz (coincidence of the dipolar and *J* coupling tensors is assumed). In panel c, the best agreement between simulation and experiment is obtained by assuming a B···P distance of 2.038 Å, the experimentally determined ^{31}P CSA parameters, and a *J* coupling anisotropy of 219 Hz.

■ CONCLUSIONS

Solid-state NMR techniques are established for the structural characterization of frustrated Lewis pairs (FLPs), especially for investigating the interactions between the Lewis acid and base functionalities. ^{11}B chemical shifts and quadrupolar coupling parameters can be interpreted in terms of the strength of the interaction between the Lewis acid and base functionality: the stronger this interaction, the lower are the ^{11}B isotropic chemical shifts and the smaller is the ^{11}B quadrupolar coupling constant. The latter result is supported by DFT calculations of electric field gradients on a GGA level for single molecules in the gas phase, which are in excellent agreement with experimentally obtained values. These DFT calculations reveal that the principal electric field gradient component, V_{zz}, is tilted about 20° away from the boron−phosphorus director. These results explain the strong B···P distance dependence of the quadrupolar coupling constant. They may also relate to the fact that it is not necessary to assume a linear orientation of H_2 in the reactive pocket of the FLP for the understanding of the mechanism of the dihydrogen activation.

$^{31}P\{^1H\}$ CPMAS NMR spectra are influenced by indirect $^{31}P-^{11}B$ spin−spin coupling, manifesting itself by asymmetric peak splittings independent of magnetic field strength. For the substituted vinylene-bridged intramolecular adducts, the experimental $^1J(^{11}B^{\cdots 31}P)$ spin−spin coupling constants extracted from these spectra are on the order of 50 Hz, in close agreement with DFT calculations. These results suggest that a significant covalent interaction is still apparent in intramolecular phosphane−borane adducts. This is also demonstrated by $^{11}B\{^{31}P\}$ REDOR and CT-REDOR experiments, which suggest the influence of non-zero contributions of the *J* coupling tensor anisotropy leading to a slightly reduced effective dipolar coupling constant. Analysis of REDOR curves assuming ΔJ = 0 leads to a systematic overestimation of the boron−phosphorus distance (by up to 0.1 Å in some cases). If *J* anisotropies on the order of 100 Hz are taken into consideration, however, the REDOR curves are well reproduced based on the crystallographic boron−phosphorus distances. With these considerations in mind, the method lends itself to distance measurements in intramolecular adducts with unknown crystal structures or amorphous materials. Overall, the present study illustrates the power and potential of solid-state NMR techniques characterizing the weak bonding interactions within boron/phosphorus-based FLPs.

In summary, we conclude that "frustration" in FLP chemistry does not mean the complete suppression of covalent interactions between the Lewis acid and base centers. As a matter of fact, the residual electron density between the reaction centers may be a necessary requirement for the typical FLP behavior. To explore whether and how the communication between these functionalities may explain the remarkable cooperative reaction behavior, ongoing NMR and DFT studies are directed toward characterizing the intermediate steps of the H_2 activation process.

■ ASSOCIATED CONTENT

Supporting Information

Complete ref 43, synthesis and general characterization of compounds **1**−**12**, and additional solid-state NMR and DFT details. This material is available free of charge via the Internet at http://pubs.acs.org.

■ AUTHOR INFORMATION

Corresponding Author

eckerth@uni-muenster.de; erker@uni-muenster.de; grimme@thch.uni-bonn.de

■ ACKNOWLEDGMENTS

This work was supported by the SFB 858 "Cooperative Systems in Chemistry". T.W. thanks the Fonds der Chemischen Industrie for a research fellowship. He acknowledges additional support by the NRW Forschungsschule "Molecules and Materials" and also thanks Dipl.-Chem. Birgitta Schirmer and Dr. Thomas Echelmeyer for helpful discussions. We cordially thank Dr. M. Sajid for providing us with a sample of compound **8**.

■ REFERENCES

(1) Stephan, D. W.; Erker, G. *Angew. Chem., Int. Ed.* **2010**, *49*, 46.
(2) Lewis, G. N. *Valence and the Structure of Atoms and Molecules*; Chemical Catalogue Company: New York, 1923.
(3) Stephan, D. W. *Dalton Trans.* **2009**, 3129.
(4) Welch, G. C.; Stephan, D. W. *J. Am. Chem. Soc.* **2007**, *129*, 1880.

(5) Welch, G. C.; Juan, R. R. S.; Masuda, J. D.; Stephan, D. W. *Science* **2006**, *314*, 1124.
(6) Spies, P.; Erker, G.; Kehr, G.; Bergander, K.; Fröhlich, R.; Grimme, S.; Stephan, D. W. *Chem. Commun.* **2007**, 5072.
(7) Spies, P.; Kehr, G.; Bergander, K.; Wibbeling, B.; Fröhlich, R.; Erker, G. *Dalton Trans.* **2009**, 1534.
(8) Mömming, C. M.; Otten, E.; Kehr, G.; Fröhlich, R.; Grimme, S.; Stephan, D. W.; Erker, G. *Angew. Chem., Int. Ed.* **2009**, *48*, 6643.
(9) Moebs-Sanchez, S.; Bouhadir, G.; Saffon, N.; Maron, L.; Bourissou, D. *Chem. Commun.* **2008**, 3435.
(10) Mömming, C. M.; Kehr, G.; Wibbeling, B.; Fröhlich, R.; Erker, G. *Dalton Trans.* **2010**, *39*, 7556.
(11) McCahill, J. S. J.; Welch, G. C.; Stephan, D. W. *Angew. Chem., Int. Ed.* **2007**, *46*, 4968.
(12) Mömming, C. M.; Frömel, S.; Kehr, G.; Fröhlich, R.; Grimme, S.; Erker, G. *J. Am. Chem. Soc.* **2009**, *131*, 12280.
(13) Ullrich, M.; Seto, K. S. H.; Lough, A. J.; Stephan, D. W. *Chem. Commun.* **2009**, 2335.
(14) Dureen, M. A.; Stephan, D. W. *J. Am. Chem. Soc.* **2009**, *131*, 8396.
(15) Cardenas, A. J. P.; Culotta, B. J.; Warren, T. H.; Grimme, S.; Stute, A.; Fröhlich, R.; Kehr, G.; Erker, G. *Angew. Chem., Int. Ed.* **2011**, *50*, 7567.
(16) Ekkert, O.; Kehr, G.; Fröhlich, R.; Erker, G. *J. Am. Chem. Soc.* **2011**, *133*, 4610.
(17) Rokob, T. A.; Hamza, A.; Stirling, A.; Soós, T.; Pápai, I. *Angew. Chem., Int. Ed.* **2008**, *47*, 2435.
(18) Hamza, A.; Stirling, A.; András Rokob, T.; Pápai, I. *Int. J. Quantum Chem.* **2009**, *109*, 2416.
(19) Grimme, S.; Kruse, H.; Goerigk, L.; Erker, G. *Angew. Chem., Int. Ed.* **2010**, *49*, 1402.
(20) Bryce, D. L.; Wasylishen, R. E.; Gee, M. *J. Phys. Chem. A* **2001**, *105*, 3633.
(21) Autschbach, J.; Zheng, S.; Schurko, R. W. *Concepts Magn. Reson., Part A* **2010**, *36A*, 84.
(22) Adiga, S.; Aebi, D.; Bryce, D. L. *Can. J. Chem.* **2007**, *85*, 496.
(23) Gullion, T.; Schaefer, J. *J. Magn. Reson.* **1989**, *81*, 196.
(24) Spies, P.; Fröhlich, R.; Kehr, G.; Erker, G.; Grimme, S. *Chem.—Eur. J.* **2008**, *14*, 333.
(25) Axenov, K. V.; Mömming, C. M.; Kehr, G.; Fröhlich, R.; Erker, G. *Chem.—Eur. J.* **2010**, *16*, 14069.
(26) Jacobsen, H.; Berke, H.; Döring, S.; Kehr, G.; Erker, G.; Fröhlich, R.; Meyer, O. *Organometallics* **1999**, *18*, 1724.
(27) Massey, A. G.; Park, A. J. *J. Organomet. Chem.* **1964**, *2*, 245.
(28) Ekkert, O.; Kehr, G.; Fröhlich, R.; Erker, G. *Chem. Commun.* **2011**, *47*, 10482.
(29) Massey, A. G.; Park, A. J.; Stone, F. G. A. *Proc. Chem. Soc.* **1963**, 212.
(30) Bennett, A. E.; Rienstra, C. M.; Auger, M.; Lakshmi, K. V.; Griffin, R. G. *J. Chem. Phys.* **1995**, *103*, 6951.
(31) Medek, A.; Harwood, J. S.; Frydman, L. *J. Am. Chem. Soc.* **1995**, *117*, 12779.
(32) Amoureux, J.-P.; Fernandez, C.; Steuernagel, S. *J. Magn. Reson., Ser. A* **1996**, *123*, 116.
(33) Massiot, D.; Fayon, F.; Capron, M.; King, I.; Le Calvé, S.; Alonso, B.; Durand, J.-O.; Bujoli, B.; Gan, Z.; Hoatson, G. *Magn. Reson. Chem.* **2002**, *40*, 70.
(34) Peersen, O. B.; Wu, X. L.; Kustanovich, I.; Smith, S. O. *J. Magn. Reson., Ser. A* **1993**, *104*, 334.
(35) Thakur, R. S.; Kurur, N. D.; Madhu, P. K. *Chem. Phys. Lett.* **2006**, *426*, 459.
(36) Vinod Chandran, C.; Madhu, P. K.; Kurur, N. D.; Bräuniger, T. *Magn. Reson. Chem.* **2008**, *46*, 943.
(37) Gullion, T.; Baker, D. B.; Conradi, M. S. *J. Magn. Reson.* **1990**, *89*, 479.
(38) Echelmeyer, T.; van Wüllen, L.; Wegner, S. *Solid State Nucl. Magn. Reson.* **2008**, *34*, 14.
(39) Bak, M.; Rasmussen, J. T.; Nielsen, N. C. *J. Magn. Reson.* **2000**, *147*, 296.
(40) Bak, M.; Nielsen, N. C. *J. Magn. Reson.* **1997**, *125*, 132.
(41) Ahlrichs, R.; Furche, F.; Hättig, C. *TURBOMOLE*, version 6.0/6.3, Universität Karlsruhe, 2009.
(42) Ahlrichs, R.; Bär, M.; Häser, M.; Horn, H.; Kölmel, C. *Chem. Phys. Lett.* **1989**, *162*, 165.
(43) Frisch, M. J. et al. *Gaussian 09*; Gaussian, Inc., Wallingford, CT, 2009.
(44) Tao, J.; Perdew, J. P.; Staroverov, V. N.; Scuseria, G. E. *Phys. Rev. Lett.* **2003**, *91*, No. 146401.
(45) Grimme, S.; Antony, J.; Ehrlich, S.; Krieg, H. *J. Chem. Phys.* **2010**, *132*, No. 154104.
(46) Weigend, F.; Ahlrichs, R. *Phys. Chem. Chem. Phys.* **2005**, *7*, 3297.
(47) Treutler, O.; Ahlrichs, R. *J. Chem. Phys.* **1995**, *102*, 346.
(48) Eichkorn, K.; Treutler, O.; Öhm, H.; Häser, M.; Ahlrichs, R. *Chem. Phys. Lett.* **1995**, *240*, 283.
(49) Eichkorn, K.; Weigend, F.; Treutler, O.; Ahlrichs, R. *Theor. Chim. Acta* **1997**, *97*, 119.
(50) Kaupp, M.; Bühl, M.; Malkin, V. G. *Calculation of NMR and EPR parameters*; Wiley-VCH: Weinheim, Germany, 2004.
(51) Grimme, S. *J. Comput. Chem.* **2006**, *27*, 1787.
(52) Feller, D. *J. Comput. Chem.* **1996**, *17*, 1571.
(53) Schuchardt, K. L.; Didier, B. T.; Elsethagen, T.; Sun, L.; Gurumoorthi, V.; Chase, J.; Li, J.; Windus, T. L. *J. Chem. Inf. Model.* **2007**, *47*, 1045.
(54) Woon, D. E.; Dunning, T. H. *J. Chem. Phys.* **1995**, *103*, 4572.
(55) Peterson, K. A.; Dunning, T. H. *J. Chem. Phys.* **2002**, *117*, 10548.
(56) Pennington, W. T. *J. Appl. Crystallogr.* **1999**, *32*, 1028.
(57) Ditchfield, R. *Mol. Phys.* **1974**, *27*, 789.
(58) Becke, A. D. *J. Chem. Phys.* **1993**, *98*, 5648.
(59) Stephens, P. J.; Devlin, F. J.; Chabalowski, C. F.; Frisch, M. J. *J. Phys. Chem.* **1994**, *98*, 11623.
(60) Becke, A. D. *Phys. Rev. A* **1988**, *38*, 3098.
(61) Perdew, J. P. *Phys. Rev. B* **1986**, *34*, 7406.
(62) Antol, I.; Glasovac, Z.; Eckert-Maksic, M. *New J. Chem.* **2004**, *28*, 880.
(63) Onak, T.; Landesman, H.; Williams, R.; Shapiro, I. *J. Phys. Chem.* **1959**, *63*, 1533.
(64) Buehl, M.; Schleyer, P. v. R. *J. Am. Chem. Soc.* **1992**, *114*, 477.
(65) Onak, T.; Diaz, M.; Barfield, M. *J. Am. Chem. Soc.* **1995**, *117*, 1403.
(66) Schäfer, A.; Huber, C.; Ahlrichs, R. *J. Chem. Phys.* **1994**, *100*, 5829.
(67) Wiberg, K. B. *Tetrahedron* **1968**, *24*, 1083.
(68) Glendering, E. D.; Reed, A. E.; Carpenter, J. E.; Weinhold, F. *NBO*, version 3.1.
(69) Massiot, D.; Fayon, F.; Deschamps, M.; Cadars, S.; Florian, P.; Montouillout, V.; Pellerin, N.; Hiet, J.; Rakhmatullin, A.; Bessada, C. *C. R. Chim.* **2010**, *13*, 117.
(70) Olivieri, A. *J. Am. Chem. Soc.* **1992**, *114*, 5758.
(71) Harris, R. K.; Olivieri, A. C. *Prog. Nucl. Magn. Reson. Spectrosc.* **1992**, *24*, 435.
(72) Moran, K. L.; Gier, T. E.; Harrison, W. T. A.; Stucky, G. D.; Eckert, H.; Eichele, K.; Wasylishen, R. E. *J. Am. Chem. Soc.* **1993**, *115*, 10553.
(73) Lindner, E.; Fawzi, R.; Mayer, H. A.; Eichele, K.; Pohmer, K. *Inorg. Chem.* **1991**, *30*, 1102.
(74) Brunklaus, G.; Chan, J. C. C.; Eckert, H.; Reiser, S.; Nilges, T.; Pfitzner, A. *Phys. Chem. Chem. Phys.* **2003**, *5*, 3768.
(75) Scheer, M.; Gregoriades, L.; Bai, J.; Sierka, M.; Brunklaus, G.; Eckert, H. *Chem.—Eur. J.* **2005**, *11*, 2163.
(76) Tang, J. A.; Ellis, B. D.; Warren, T. H.; Hanna, J. V.; Macdonald, C. L. B.; Schurko, R. W. *J. Am. Chem. Soc.* **2007**, *129*, 13049.
(77) Eichele, K.; Wasylishen, R. E.; Corrigan, J. F.; Doherty, S.; Carty, A. J.; Sun, Y. *Inorg. Chem.* **1993**, *32*, 121.
(78) Eichele, K.; Wasylishen, R. E.; Maitra, K.; Nelson, J. H.; Britten, J. F. *Inorg. Chem.* **1997**, *36*, 3539.
(79) Power, W. P. *J. Am. Chem. Soc.* **1995**, *117*, 1800.
(80) Ashbrook, S. E.; Dowell, N. G.; Prokes, I.; Wimperis, S. *J. Am. Chem. Soc.* **2006**, *128*, 6782.

(81) Harris, R. K.; Becker, E. D.; Cabral de Menezes, S. M.; Goodfellow, R.; Granger, P. *Pure Appl. Chem.* **2001**, *73*, 1795.
(82) Huffman, J. C.; Skupinski, W. A.; Caulton, K. G. *Cryst. Struct. Commun.* **1982**, *11*, 1435.
(83) Karplus, M. *J. Am. Chem. Soc.* **1963**, *85*, 2870.
(84) Karplus, M. *J. Chem. Phys.* **1959**, *30*, 11.
(85) Foster, J. P.; Weinhold, F. *J. Am. Chem. Soc.* **1980**, *102*, 7211.
(86) Reed, A. E.; Weinhold, F. *J. Chem. Phys.* **1983**, *78*, 4066.
(87) Chan, J. C. C.; Eckert, H. *J. Magn. Reson.* **2000**, *147*, 170.
(88) Mitchell, D. J.; Evans, J. N. S. *Chem. Phys. Lett.* **1998**, *292*, 656.
(89) Elbers, S.; Strojek, W.; Koudelka, L.; Eckert, H. *Solid State Nucl. Magn. Reson.* **2005**, *27*, 65.
(90) Strojek, W.; Fehse, C. M.; Eckert, H.; Ewald, B.; Kniep, R. *Solid State Nucl. Magn. Reson.* **2007**, *32*, 89.
(91) Raskar, D. B.; Eckert, H.; Ewald, B.; Kniep, R. *Solid State Nucl. Magn. Reson.* **2008**, *34*, 20.